

Long-range and hierarchical language predictions in brains and algorithms

Charlotte Caucheteux^{1,2}, Alexandre Gramfort², and Jean-Rémi King^{1,3}

¹Facebook AI Research, Paris, France; ²Université Paris-Saclay, Inria, CEA, Palaiseau, France; ³École normale supérieure, PSL University, CNRS, Paris, France

Deep learning has recently made remarkable progress in natural language processing. Yet, the resulting algorithms remain far from competing with the language abilities of the human brain. Predictive coding theory offers a potential explanation to this discrepancy: while deep language algorithms are optimized to predict adjacent words, the human brain would be tuned to make long-range and hierarchical predictions. To test this hypothesis, we analyze the fMRI brain signals of 304 subjects each listening to ≈ 70 min of short stories. After confirming that the activations of deep language algorithms linearly map onto those of the brain, we show that enhancing these models with long-range forecast representations improves their brain-mapping. The results further reveal a hierarchy of predictions in the brain, whereby the fronto-parietal cortices forecast more abstract and more distant representations than the temporal cortices. Overall, this study strengthens predictive coding theory and suggests a critical role of long-range and hierarchical predictions in natural language processing.

Natural Language Processing | functional Magnetic Resonance Imaging
| Predictive coding

In less than three years, deep learning has made considerable progress in text generation, translation and completion (1–4) thanks to algorithms trained with a simple learning rule: predicting words from their adjacent context. Remarkably, the activations of these models have been shown to linearly map onto human brain responses to speech and text (5–9). Besides, this mapping appears to primarily depend on the algorithms’ ability to predict future words (7, 8), hence suggesting that this learning rule suffices to make them converge to brain-like computations.

Yet, a major gap remains between humans and these algorithms: current language models are still poor at story generation and summarization as well as dialogue and question answering (10–14); they fail to capture many syntactic constructs and semantics properties (15–19), and their linguistic understanding is often superficial (16, 18–20).

Predictive coding theory (21–23) offers a potential explanation to these shortcomings: while deep language models are tuned to predict the very next word, this theory suggests that the human brain predicts (i) long-range and (ii) hierarchical representations (Figure 1A). Previous work has already evidenced speech predictions in the brain, by correlating word or phonetic surprisal with functional Magnetic Resonance Imaging (fMRI) (24–27), electroencephalography (28, 29), magnetoencephalography (30) and electrocorticography (9, 31). However, such surprisal estimates derive from models trained to predict the very next token (i.e. word *or* phoneme), and reduce down their output to a single number: the probability of the next token. Consequently, (i) the nature of the predicted multivariate representations as well as (ii) their temporal scope remain largely unknown.

Here, we address these issues by analyzing the brain signals of 304 subjects listening to short stories, while their brain activity was recorded with fMRI (32). First, we confirm that deep language algorithms linearly map onto brain activity (6, 8, 33). Then, we show that adding long-range and hierarchical predictions improves such mapping. After confirming that the activations of deep language algorithms linearly map onto brain activity (6, 8, 33), we show that enhancing these models with long-range and hierarchical predictions improves their brain mapping. Critically, and in line with predictive coding theory, our results reveal a hierarchical organization of language prediction in the cortex, in which the highest stages forecast (i) the most distant and (ii) the most abstract representations.

Results

Deep language models map onto brain activity. First, we quantify the similarity between deep language models and the brain, when these two systems are input with the same stories. For this, we use the Narratives dataset* (32), and analyze the fMRI of 304 subjects listening to ≈ 70 min of short stories. We then fit, for each voxel and each subject independently, a linear ridge regression to predict the fMRI signals from the activations of a variety of deep language models. Finally, we compute the corresponding “brain scores” using held-out data, i.e. the voxel-wise correlation between (i) the fMRI signals and (ii) the predictions of the ridge regression input with the activations of a given language model (Figure 1B). For clarity, we first focus on the activations of the eighth layer of GPT-2 provided by HuggingFace† (2), as it has been shown to best predict brain activity (7, 8).

In line with previous studies (5, 7, 33, 34), the activations of GPT-2 accurately map onto a distributed and bilateral set of brain areas. Brain scores peak in the auditory cortex, as well as in the anterior temporal and superior temporal areas (Figure 2A and Figure S8). The effect sizes of these brain scores are in line with previous work (7, 35, 36): for instance, the highest brain scores ($R = 0.23$, in the superior temporal sulcus (Figure 2A) represent 60% of the maximum explainable signal, as assessed with a shared-response model across subjects (SI.O and Figure S7). Figure S5 shows that, on average, similar brain scores are achieved with other state-of-the-art language models.

Overall, these results confirm that deep language models linearly map onto brain responses to spoken stories.

Tracking long-range forecast in the brain. We then test whether enhancing language models with forecast representations leads

*<https://openneuro.org/datasets/ds002345/versions/1.1.4>.

†<https://huggingface.co/>

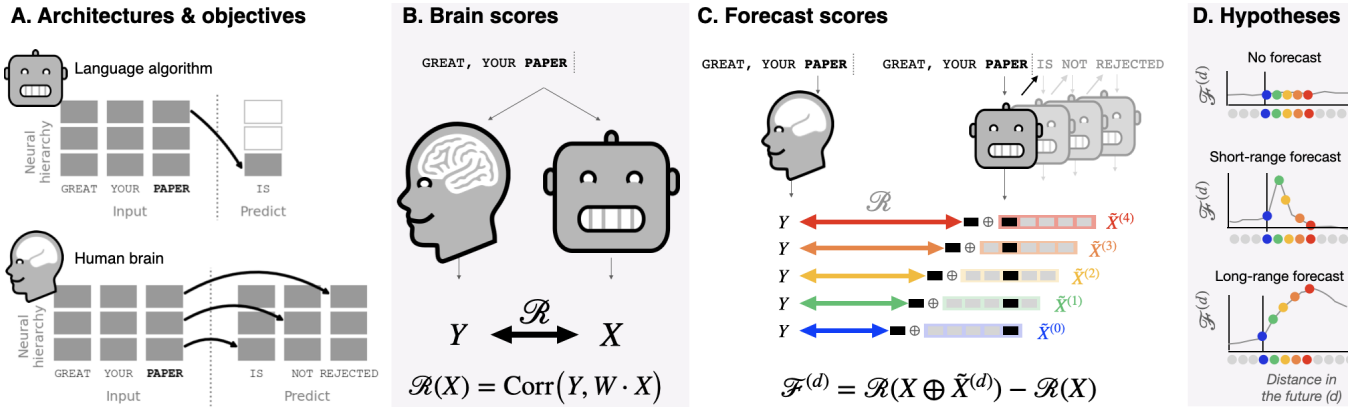


Fig. 1. Approach. **A.** Deep language algorithms are typically trained to predict words from their close contexts. Unlike these algorithms, the brain makes, according to predictive coding theory, (i) long-range and (ii) hierarchical predictions. **B.** To test this hypothesis, we first extract the fMRI signals of 304 subjects each listening to ≈ 70 min of short stories (Y) as well as the activations of a deep language algorithm (X) input with the same stories. We then quantify the similarity between X and Y with a “brain score”: a Pearson correlation \mathcal{R} after an optimal linear projection W (Methods D). **C.** To test whether adding representations of future (or predicted, see Figure S6) words improves this correlation, we concatenate (\oplus) the network’s activations (X , depicted here as a black rectangle) to the activations of a “forecast window” (\tilde{X} , depicted here as a colored rectangle). We use principal component analysis to reduce the dimensionality of the forecast window down to the dimensionality of X . Finally, \mathcal{F} quantifies the gain of brain score obtained by enhancing the activations of the language algorithm to this forecast window. We repeat this analysis with variably distant windows (d , Methods E). **D.** A flat forecast score across distances would indicate that forecast representations do not make the algorithm more similar to the brain (top). By contrast, a forecast score peaking at $d > 1$ (bottom) would indicate that the model lacks brain-like forecast. The peak of \mathcal{F}^d indicates how far off in the future the algorithm would need to forecast representations to be most similar to the brain.

to higher brain scores (Figure 1D). Specifically, for each word, we concatenate (i) the model activations of the present word (denoted X) and (ii) a “forecast window” (denoted $\tilde{X}^{(d)}$), consisting of the embeddings of future words. This forecast window is parameterized by a variable distance d and a fixed width (seven words, see SI.N for the growing window analysis). For each distance d , we compute the “forecast score” (denoted \mathcal{F}^d) by comparing the brain scores obtained with and without the forecast representations (Figure 2B).

Our results show that \mathcal{F} is maximal for a distance of $d = 8$ words, and peaks in the areas typically associated with language processing (Figure 2B-D). These forecast scores are bilaterally distributed in the brain, at the exception of the infero-frontal ($p < 10^{-5}$ in Pars Opercularis, using a pairwise Wilcoxon test between the left and right hemispheres) and supramarginal gyri ($p < 10^{-9}$), which exhibit a significant lateralization effect (Figure S8B).

Supplementary analyses confirm that (i) forecast representations are best captured with a window size of ≈ 8 words, (ii) random forecast representations do not improve the brain scores, and (iii) using the words generated by GPT-2 instead of the true future words achieve lower but similar results (SI.N).

Together, these results reveal long-range forecast representations in the brain, which represents a 23% ($\pm 9\%$ across subjects) improvement in brain scores (Figure 2AB).

Forecast distance varies along the cortical hierarchy. Do all brain regions predict the same time window? To address this issue, we estimate the peak of the forecast score of each voxel and denote d^* the corresponding distance. The results show that the prefrontal areas forecast, on average, further off in the future than temporal areas (Figure 2E). For instance, d^* in the inferior temporal gyrus (ITG) is higher than in the anterior superior temporal sulcus (aSTS) ($\Delta d^* = 0.9 \pm 0.2, p < 10^{-4}$, Figure 2F and G). The variation of optimal forecast distance along the temporo-parieto-frontal hierarchy is largely symmetric across the two hemispheres (Figure S8).

Forecast depth varies along the cortical hierarchy. What is the nature of these forecast representations? To address this issue, we assess whether forecast representations relate to (i) shallow or deep as well as (ii) syntactic or semantic representations. To this aim, we first compute the forecast scores similarly as in Figure 1C, but now vary the layer used from GPT-2. Then, we identify k^* for each voxel *i.e.* the depth that maximizes the forecast scores (Methods H).

Our results show that the optimal forecast depth varies along the expected cortical hierarchy (Figure 3A). Specifically, associative cortices are best modeled with deeper forecasts ($k^* > 6$) than low-level language areas (*e.g.* $k^* < 6$ in Heschel’s gyri/sulci, anterior STS, Figure 3A-B). The difference between regions, while small on average, is highly significant across subjects (*e.g.* between the angular and Heschel’s gyri: $\Delta k^* = 2.5 \pm 0.3, p < 10^{-12}$), and observed in both the left and right hemispheres (Figure 3B).

Together, these results suggest that the long-range forecasts of fronto-parietal cortices are more abstract than the short-term forecasts of low-level brain regions.

Short and long range forecasts target syntactic and semantic representations, respectively. To decompose forecast representations into syntactic and semantic components, we apply a method introduced in (33) and proceed as follows: for each word and its preceding context, we generate ten possible futures which matches the syntax of the true future words. For each of these possible futures, we extract the corresponding GPT-2 activations, and average them across the ten possible futures (Figure 4A, Methods I). As explained in (33), this method allows us to decompose the activations of a given language model X into syntactic (the average vector, denoted X_{syn}) and semantic components (the residuals, $X_{\text{sem}} = X - X_{\text{syn}}$).

Once the syntactic and semantic forecast windows are built, we compute the corresponding forecast scores (Methods J). The results show that semantic forecasts are long-range and involve a distributed network peaking in the frontal and

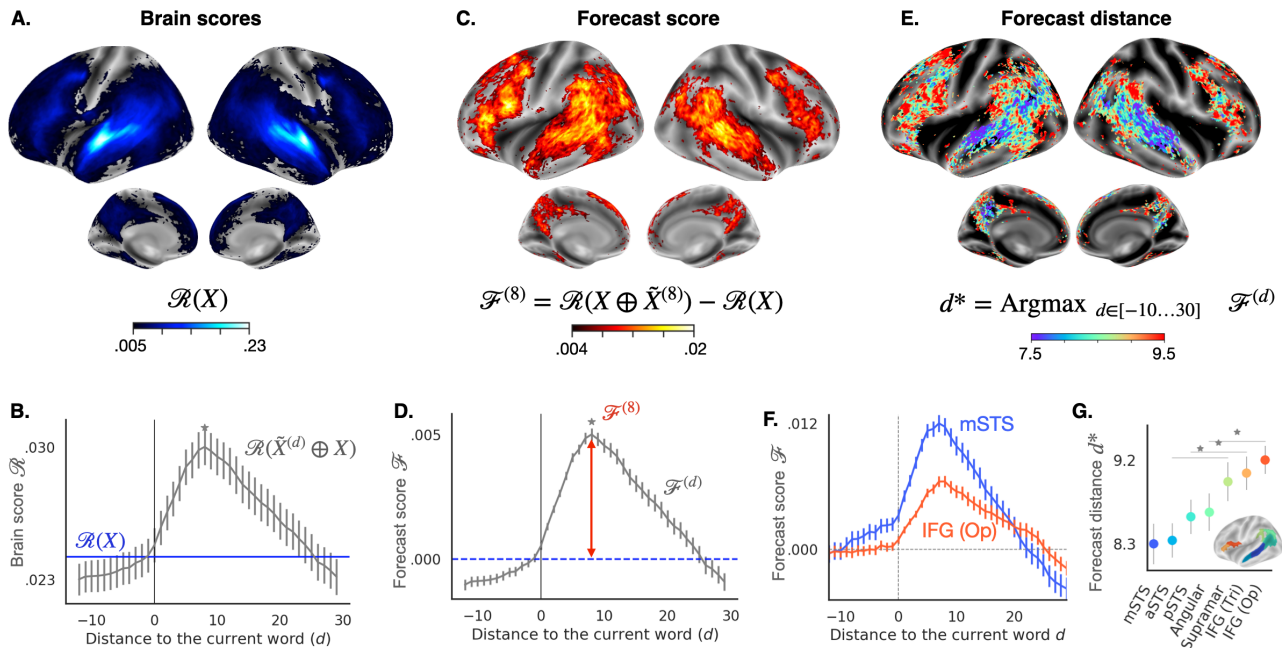


Fig. 2. Long-range forecasts in the brain. **A.** The “brain score” (\mathcal{R} , Figure 1B, Methods D), obtained with GPT-2, for each subject and each voxel, and here averaged across subjects ($n=304$). Only the voxels with significant brain scores are color-coded. **B.** Average (across voxels) brain scores obtained with GPT-2 with (grey) or without (blue) forecast representations. The average brain score peaks at $d^* = 8$ (grey star). **C.** For each voxel, the average (across subjects) “forecast score” \mathcal{F}^d , *i.e.* the gain in brain score when concatenating the activations of GPT-2 with a forecast window $\tilde{X}^{(8)}$. Only the voxels with significant forecast scores are color-coded. **D.** Average (across voxels) forecast scores for different distance d . **E.** Distance that maximizes \mathcal{F}^d , computed for each subject and each voxel, and denoted d^* . This “forecast distance” reveals the regions associated with short- and long-range forecasts. Regions in red and blue are associated with long-range and short-range forecasts, respectively. We only display the voxels with a significant average peak ($\mathcal{F}^{d^*} - \mathcal{F}^0$, $d^* = 8$, cf. Methods G). **F.** Same as D. but for two selected regions of the brain: the middle superior temporal sulcus (mSTS) and the pars opercularis of the inferior frontal gyrus (IFG-Op). **G.** Forecast distance of seven regions of interest, as computed for each voxel of each subject and then averaged within the selected brain regions. For all panels, the error bars are SEM across subjects. All brain maps are thresholded at $p < .01$, as assessed with a FDR-corrected two-sided Wilcoxon test across subjects.

parietal lobes. By contrast, syntactic forecasts (Figure 4B) are relatively short-range and localized in the superior temporal and left frontal areas (Figure 4C and D).

Overall, these results reveal a hierarchy of predictions in the brain in which the superior temporal cortex forecast short-term, shallow and syntactic representations whereas the infero-frontal and parietal areas forecast long-term, abstract and semantic representations.

Discussion

In the present study, we put specific hypotheses of predictive coding theory to the test (21–23): while deep language algorithms are typically trained to make (i) adjacent and (ii) word-level predictions (1–3, 37–39), we assess whether the human brain predicts (i) long-distance and (ii) hierarchical representations. To this aim, we capitalize on the success of a recent methodology (40–43) and compare the activations of the brain to those of state-of-the-art deep language models (5–7, 35, 44). We successfully validate our hypothesis on a large cohort of 304 subjects listening to 70 min of spoken narratives (32): brain activity is best explained by deep language algorithms enhanced with long-range and hierarchical forecasts. Our study provides three additional contributions.

Long-range predictions. First, the cortical regions repeatedly linked to high-level semantics, long-term planning, attentional control, abstract thinking and other high-level executive functions (45, 46), namely, the lateral, dorso-lateral and infero-frontal cortices, as well as the supra-marginal gyrus, here

exhibit the longest forecast distances. This result echoes with previous studies showing that the integration constant of the fronto-parietal cortices is larger than those of sensory and temporal areas (47–50). Specifically, our study suggests that these regions, located at the top of the language hierarchy, are not limited to passively integrating past stimuli, but actively anticipate future language representations.

Hierarchical predictions. Second, we show that the depth of forecast representations varies along a similar anatomical organization: the superior temporal sulcus and gyrus are best modeled with low-level forecast representations as compared to the middle temporal, parietal and frontal areas. This finding extends previous studies investigating the multiplicity of predictions underlying complex sound or speech processing (28, 29, 51): while previous works focused on correlating brain activity with a subset of hand-crafted and unidimensional prediction errors (e.g. word or phoneme surprisal), the present analyses explore, and can thus decompose high-dimensional predictions. More generally, our results support the idea that, unlike current language algorithms, the brain is not limited to predict word-level representations, but rather makes hierarchical predictions.

Syntactic and semantic predictions. Finally, we use a recent method to decompose these neural activations into syntactic and semantic representations (33), and show that the long-range forecasts are predominantly driven by semantic features. This finding strengthens the idea that while syntax may be explicitly represented in neural activity (52, 53), predicting

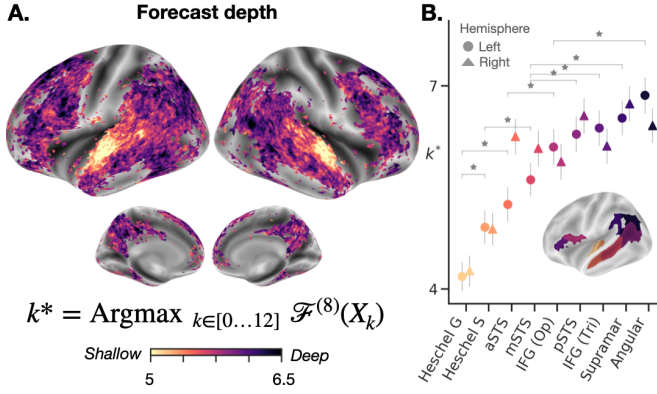


Fig. 3. Hierarchical forecasts in the brain **A.** Depth of the representation that maximizes the forecast score in the brain, denoted k^* . Forecast scores are computed for each depth, subject and voxel, at a fix distance $d^* = 8$ and averaged across subjects. We compute the optimal depth for each subject and voxel and plot the average forecast depth across subjects. Dark regions are best accounted for by deep forecasts, while light regions are best accounted for by shallow forecasts. Only significant voxels are color-coded, following Figure 2C). **B.** Same as A, with k^* averaged across the voxels of nine regions of interest, in the left (circle) and right (triangle) hemispheres. Error bars are SEM across subjects. Pairwise significance between regions is assessed using a two-sided Wilcoxon test on the left hemisphere’s scores ($p < .05$).

high-level meaning may be at the core of language processing (54, 55).

On the potential benefit of a predicting coding architecture. Together, these results support predictive coding theories, whereby the brain continually predicts sensory inputs, compares these predictions to the truth, and updates its internal model accordingly (21, 22, 56). Our study further clarifies this general framework: not only does the brain predict sensory inputs, but each level of the cortical hierarchy appears to be organized to predict different temporal scopes and different levels of abstraction (Figure 1A).

This computational organization is at odd with current language algorithms which are trained to make adjacent and word-level predictions (Figure 1A). We speculate that the brain architecture evidenced in this study presents at least one major benefit over its deep learning counter-parts: while future observations rapidly become indeterminate in their original format, their latent and abstract representations may remain predictable over long time periods. This issue is already pervasive in speech- and image-based algorithms and has been partially bypassed with losses based on pretrained embedding (57), contrastive learning and, more generally, joint embedding architectures (58–61). Here, we highlight that this issue also prevails in language models, where word sequences – but arguably not their meaning – rapidly become unpredictable. Our results suggests that predicting hierarchical representations over multiple temporal scopes may be critical to address the indeterminate nature of such distant observations.

Beyond clarifying the the brain and computational bases of language, our study thus calls for training algorithms to predict a hierarchical representation of future inputs.

Materials and Methods

A. Notations. We denote:

- w a sequence of M words (here, several short stories).
- X the activations of a deep language model input with w , of size $M \times U$, with U the dimensionality of the embeddings (for a layer of GPT-2, $U = 768$). Except if stated otherwise, we use the activations extracted from the eighth layer of a 12-layer GPT-2 model (Methods C). We will explicitly denote X_k the activations extracted from layer k when using another layer.
- Y the fMRI recordings elicited by w , of size $T \times V$, with T the number of fMRI time samples, and V the number of voxels (Methods B).
- $\mathcal{R}(X)$ the brain score of X (Methods D).
- $\tilde{X}^{(d)}$ the forecast window containing information up to d words in the future. In short, the forecast window is the concatenation of the deep net activations of seven successive words, the last word being at a distance d from the current word (Methods E).
- $\mathcal{F}^{(d)}(X)$, the forecast score at distance d , i.e. the gain in brain score when concatenating the forecast window $\tilde{X}^{(d)}$ to the network’s activations; $\mathcal{F}^{(d)}(X) = \mathcal{R}(X \oplus \tilde{X}^{(d)}) - \mathcal{R}(X)$ (Methods G).
- d^* , the distance maximizing the forecast score; $d^* = \operatorname{argmax}_{d \in [-10, \dots, 30]} \mathcal{F}^{(d)}(X)$ (Methods G).
- k^* , the network’s depth maximizing the forecast score at a fixed distance $d = 8$; $k^* = \operatorname{argmax}_{k \in [0, \dots, 12]} \mathcal{F}^{(8)}(X_k)$, with X_k the activations extracted from the k^{th} layer of GPT-2. We use $d = 8$ because it is the distance with the best forecast score on average across subjects and voxels (Methods H).

B. fMRI dataset. We use the brain recordings (denoted Y) of the “Narratives” dataset (32), a publicly available dataset containing the fMRI recordings of 345 subjects listening to 27 spoken stories in English, from ≈ 3 min to ≈ 56 min (≈ 4.6 h of unique stimulus in total). We use the pre-processed fMRI signals from the original dataset, without spatial smoothing (referred to as “afni-nosmooth” in the repository) and sampled with $\text{TR} = 1.5$ s: the preprocessing steps were performed using fMRIPrep (62), no temporal filtering was applied. The resulting preprocessing leads to the analysis of cortical voxels projected onto the surface and morphed onto a “fsaverage” template brain, and hereafter referred to as voxels simplicity. As suggested in the original paper, some subject-story pairs were excluded because of noise, resulting in 622 subject-story pairs and 4 h of unique audio material in total.

C. Deep language models’ activations. We compare the fMRI recordings with the activations of a variety of pretrained deep language model input with the same sentences presented to the subjects. For clarity, we primarily focus on GPT-2, a high-performing language model trained to predict words given their previous context. GPT-2 consists of twelve Transformer modules (1, 2), each of them referred to as “layer”, stacked onto one non-contextual word embedding layer. Here, we use the pre-trained models from Huggingface (63) (1.5 billion parameters, trained on 8 million web pages) (c.f. SI N for the other deep language models).

In practice, to extract the activations X elicited by a sequence of M words w , from the k^{th} layer of the network, we 1) format the textual transcript of the sequence w (replacing special punctuation marks such as “-” and duplicated marks “?” by dots) 2) tokenize the text using Huggingface tokenizer, 3) input the network with the tokens and 4) extract the corresponding activations from layer k . This results in a vector of size $M \times U$, with M the number of words and U the number of units per layer (here $U = 768$). Given the constrained context size of the network, each word is successively input to the network with at most 1024 previous tokens. For instance, while the third word’s vector is computed by inputting the network with (w_1, w_2, w_3) , the last word’s vectors w_M is computed by inputting the network with (w_{M-1024}, \dots, w_M) . The alignment between the stories’ audio recordings and their textual transcripts was provided in the original Narratives database (32).

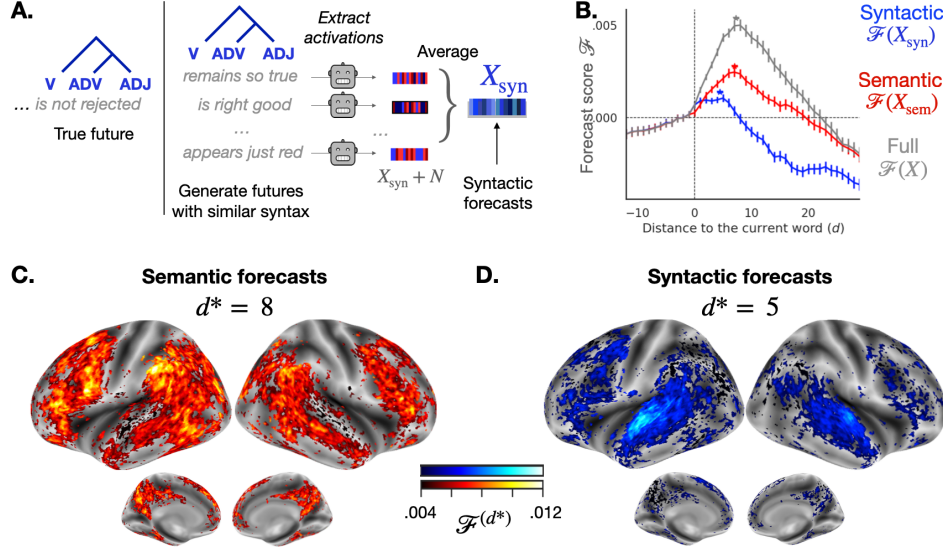


Fig. 4. Syntactic and semantic forecasts in the brain. **A.** Method to extract syntactic and semantic forecast representations, adapted from (33). For each word and its context (e.g. ‘Great, your *paper* ...’, we generate ten possible futures with the same syntax as the original sentence (part-of-speech and dependency tree) but randomly sampled semantics (e.g. ‘... remains so true’, ‘... appears so small’). Then, we extract the corresponding GPT-2 activations (layer eight). Finally, we average the activations across the ten futures. This method allows to extract the syntactic component common to the ten futures, denoted X_{syn} . The semantic component is defined as the residuals of syntax in the full activations; $X_{\text{sem}} = X - X_{\text{syn}}$. We build the syntactic and semantic forecast windows by concatenating the syntactic and semantic components of seven consecutive future words, respectively (Methods J). **B.** Syntactic (blue) and semantic (red) forecast scores, on average across all voxels, following Figure 1C. Error bars are SEM across subjects. The average peaks across subjects is indicated with a star. **C.** Semantic forecast scores for each voxel, averaged across subjects and at $d^* = 8$, the distance that maximizes the semantic forecast scores in B. Only significant voxels are displayed similarly to Figure 2C. **D.** Same as C. for syntactic forecast scores and $d^* = 5$.

D. Brain scores. Following previous works (7, 35, 44), we evaluate, for each subject s and voxel v , the mapping between 1) the fMRI activations $Y^{(s,v)}$ in response to the audio-stories and 2) the activations X of the deep network input with the textual transcripts of the same stories. To this end, we fit a linear ridge regression W on a train set to predict the fMRI scans given the network’s activations. Then, we evaluate this mapping by computing the Pearson correlation between predicted and actual fMRI scans on a held out set:

$$\mathcal{R}^{(s,v)} : X \mapsto \text{Corr}(W \cdot X, Y^{(s,v)}) \quad , \quad [1]$$

with W the fitted linear projection, Corr Pearson’s correlation, X the activations of GPT-2 and $Y^{(s,v)}$ the fMRI scans of one subject s at one voxel v , both elicited by the same held out stories.

In practice and following (35), we model the slow build response thanks to a finite impulse response (FIR) model with 6 delays. Still following (35), we sum the model activations of the words presented within the same TR, in order to match the sampling frequency of the fMRI and the language models. Then, we estimate the linear mapping W with a ℓ_2 -penalized linear regression after standardizing the data, and reducing their dimensionality (computational reasons). We follow scikit-learn implementation (64) and use a pipeline with the following steps: standardization of the features (set to 0 mean with a standard deviation of 1 using a ‘StandardScaler’), principal component analysis (PCA) with twenty components[‡], ℓ_2 -penalized linear regression (‘RidgeCV’ in scikit-learn). The regularization hyperparameter of the ‘RidgeCV’ is selected with a nested leave-one-out cross-validation among ten possible values log-spaced between 10^{-1} and 10^8 for each voxel and each training fold.

The outer cross-validation scheme allowing for an independent performance evaluation, uses five folds obtained by splitting the fMRI time series into five contiguous chunks. The Pearson correlations averaged across the five test folds is called “brain score”, denoted $\mathcal{R}^{(s,v)}(X)$. It measures the mapping between the activation space X and the brain of one subject s at one voxel v , in response to the same language stimulus.

[‡]Twenty is the number of components corresponding to the “elbow” of the explained variance ratio when applying principal component analysis on the activations of the eighth layer of GPT-2, ‘RidgeCV’ model cross the words of the stories.

In Figure 2A and B, brain scores are computed for each (subject, voxel) pair. We then average the brain scores across subjects (Figure 2A) and/or voxels (Figure 2B) depending on the analysis. For simplicity, we denote $\mathcal{R}(X)$ the brain scores averaged across subjects and/or voxels.

E. Forecast windows. The forecast window at distance d , denoted $\tilde{X}^{(d)}$, is the concatenation of the network’s activations of seven successive words, the last one being at a distance d from the current word. Precisely, the forecast window of a word w_n , at a distance d is the concatenation of the network’s activations elicited by words $w_{n+d-7}, \dots, w_{n+d}$. Thus,

$$\tilde{X}^{(d)} = (X_{w_{n+d-7}} \oplus \dots \oplus X_{w_{n+d}})_{n \in [1, \dots, M]} \quad , \quad [2]$$

with \oplus the concatenation operator, and M the number of words in the transcript w . Note that d can be negative: in that case, the forecast window only contains past information. Except if stated otherwise, the forecast window is built out of the activations X extracted from the eighth layer of GPT-2. In Figure 3, the forecast window is built out of the activations X_k extracted from different layers k of GPT-2. We denote $\tilde{X}_k^{(d)}$ the corresponding forecast windows. In Figure 4, the forecast windows are built out of the syntactic (X_{syn}) and semantic (X_{sem}) activations of GPT-2 (cf. Methods I and J).

F. Forecast scores. For each distance d , subject s and voxel v , we compute the “forecast score” $\mathcal{F}^{(d,s,v)}$, which is the gain in brain score when concatenating the forecast windows to the present GPT-2 activations. Thus,

$$\mathcal{F}^{(d,s,v)} : X \mapsto \mathcal{R}^{(s,v)}(X \oplus \tilde{X}^{(d)}) - \mathcal{R}(X) \quad , \quad [3]$$

To match the dimensionality of X and \tilde{X} , the principal component analysis used to compute the mapping (Methods D) was trained on X and \tilde{X} separately, before concatenating the two features: i.e. $\mathcal{F}(X) = \mathcal{R}(\text{pca}(X) + \text{pca}(\tilde{X})) - \mathcal{R}(\text{pca}(X))$.

G. Forecast distance. To test whether the forecast score varies along the cortical hierarchy, we estimate the distance that maximizes the

forecast score. Precisely, the optimal “forecast distance” d^* for each subject s and voxel v is defined as:

$$d_{(s,v)}^* = \operatorname{argmax}_{d \in [-10, \dots, 30]} \mathcal{F}^{(d,s,v)}(X) , \quad [4]$$

with X the activations of the language model, $\mathcal{F}^{(d,s,v)}$ the forecast score at distance d for subject s and voxel v (Eq. (3)). The forecast distances d^* are then averaged across subjects and/or voxels depending on the analyses.

The present analysis is only relevant for the brain regions for which forecast scores are not flat. Indeed, computing the distance maximizing a flat curve would be misleading. Thus, in Figure 2E, we compute the difference $\mathcal{F}^8 - \mathcal{F}^0$ for each subject and voxel, assess the significance with Wilcoxon test across subjects, and ignore the voxels with a non-significant difference ($p > .01$).

H. Forecast’s depth. To test whether the forecast depth varies along the cortical hierarchy, we compute the forecast score for different depth of representation. Precisely, we proceed similarly as in F, but replacing X by the activations X_k extracted from layer k of GPT-2 ($k \in [0, \dots, 12]$) in Eq. (3) and Eq. (2). Then, we compute the depth maximizing the forecast score, called “forecast depth”, and given by:

$$k_{(d,s,v)}^* = \operatorname{argmax}_{k \in [0, \dots, 12]} \mathcal{F}^{(d,s,v)}(X_k) , \quad [5]$$

with $\mathcal{F}^{(d,s,v)}(X_k) = \mathcal{R}^{(s,v)}(X_k \oplus \tilde{X}_k^{(d)}) - \mathcal{R}(X_k)$ (Eq. (3)). For simplicity, we focus on the fixed distance $d = 8$ (Figure 3C and D), which maximizes the forecast score in Figure 2.

I. Decomposing the activations of language models into syntactic and semantic components. To extract the syntactic and semantic components of X , a vector of activations in response to a story w , we apply a method introduced in (33) (Figure 4A). For each word, 1) we generate $k = 10$ futures of the same syntax as the true future (*i.e.* same part-of-speech and dependency tags as the true future), but randomly sampled semantics, 2) we compute the activations for each of the ten possible futures, and 3) we average the activations across the ten futures. This method allows to extract the average vector X_{syn} , that contains syntactic information but is deprived from semantic information. The semantic activations $X_{\text{sem}} = X - X_{\text{syn}}$ are the residuals of syntax in the full activations X .

J. Syntactic and semantic forecast windows. To investigate syntactic and semantic forecasts in the brain, we build forecast windows out of the syntactic and semantic activations of GPT-2, respectively. To this aim, we first build the forecast windows out of GPT-2 activations $\tilde{X}_{\text{syn}}^{(d)}$, similarly as E. Then, we extract the syntactic $\tilde{X}_{\text{syn}}^{(d)}$ and semantic $\tilde{X}_{\text{sem}}^{(d)}$ components of the concatenated activations, as introduced in (33) and described in I. Finally, the syntactic forecast score is the increase in brain score when concatenating the syntactic window:

$$\mathcal{F}_{\text{syn}}^{(d)} = \mathcal{R}(X \oplus \tilde{X}_{\text{syn}}^{(d)}) - \mathcal{R}(X) \quad [6]$$

Similarly, the semantic forecast score is given by:

$$\mathcal{F}_{\text{sem}}^{(d)} = \mathcal{R}(X \oplus \tilde{X}_{\text{sem}}^{(d)}) - \mathcal{R}(X) \quad [7]$$

K. Brain parcellation. We systematically implement whole brain analyses and compute scores for each voxel in the brain. Yet, for simplicity, we report the scores averaged across selected regions of interest in Figure 2F,G and 3C. To this aim, we use a subdivision of the Destrieux Atlas (65). Regions with more than 500 vertices are split into smaller parts. This results in 142 regions per hemisphere, each containing less than 500 vertices. In Figure 2G and 3C, we use the following acronyms:

L. Statistical significance. We systematically implement single-subject and whole brain analyses: all metrics (brain score, forecast score, forecast distance and depth) are computed for each subject, voxel pair. We report the metrics averaged across subjects and/or voxels depending on the analysis. Statistics are computed across subjects, using the two-sided Wilcoxon test from Scipy (66) assessing whether the metric (or the difference between two metrics) is

Acronym	Definition
STG / STS	Superior temporal gyrus / sulcus
aSTS	Anterior STS
mSTS	Mid STS
pSTS	Posterior STS
Angular / Supramar	Angular / Supramarginal inferior parietal gyrus
IFG / IFS	Inferior frontal gyrus / sulcus
Tri / Op	Pars triangularis / opercularis (IFG)
Heschel G / Heschel S	Heschel gyrus / sulcus

significantly different from zero. We report an effect as significant if its p-value is lower than 0.01. Error bars systematically refer to the Standard Errors of the Means (SEM) across subjects, following Scipy implementation.

References

- Ashish Vaswani, Noam Shazeer, Niki Parmar, Jakob Uszkoreit, Llion Jones, Aidan N Gomez, Łukasz Kaiser, and Illia Polosukhin. Attention is All you Need. In *Advances in Neural Information Processing Systems*, volume 30. Curran Associates, Inc., 2017.
- Alec Radford, Jeffrey Wu, Rewon Child, David Luan, Dario Amodei, and Ilya Sutskever. Language Models are Unsupervised Multitask Learners. page 24, 2018.
- Tom B. Brown, Benjamin Mann, Nick Ryder, Melanie Subbiah, Jared Kaplan, Prafulla Dhariwal, Arvind Neelakantan, Pranav Shyam, Girish Sastry, Amanda Askell, Sandhini Agarwal, Ariel Herbert-Voss, Gretchen Krueger, Tom Henighan, Rewon Child, Aditya Ramesh, Daniel M. Ziegler, Jeffrey Wu, Clemens Winter, Christopher Hesse, Mark Chen, Eric Sigler, Mateusz Litwin, Scott Gray, Benjamin Chess, Jack Clark, Christopher Berner, Sam McCandlish, Alec Radford, Ilya Sutskever, and Dario Amodei. Language Models are Few-Shot Learners. *arXiv:2005.14165 [cs]*, July 2020. arXiv: 2005.14165.
- Angela Fan, Mike Lewis, and Yann Dauphin. Hierarchical Neural Story Generation. *arXiv:1805.04833 [cs]*, May 2018. arXiv: 1805.04833.
- Shailee Jain and Alexander G Huth. Incorporating Context into Language Encoding Models for fMRI. preprint, Neuroscience, May 2018.
- Mariya Toneva and Leila Wehbe. Interpreting and improving natural-language processing (in machines) with natural language-processing (in the brain). *arXiv:1905.11833 [cs, q-bio]*, November 2019. arXiv: 1905.11833.
- Charlotte Caucheteux and Jean-Rémi King. Language processing in brains and deep neural networks: computational convergence and its limits. *bioRxiv*, page 2020.07.03.186288, July 2020. . Publisher: Cold Spring Harbor Laboratory Section: New Results.
- Martin Schrimpf, Idan Blank, Greta Tuckute, Carina Kauf, Eghbal A. Hosseini, Nancy Kanwisher, Joshua Tenenbaum, and Evelina Fedorenko. Artificial Neural Networks Accurately Predict Language Processing in the Brain. *bioRxiv*, page 2020.06.26.174482, June 2020. . Publisher: Cold Spring Harbor Laboratory Section: New Results.
- Ariel Goldstein, Zaid Zada, Eliav Buchnik, Mariano Schain, Amy Price, Bobbi Aubrey, Samuel A. Nastase, Amir Feder, Dotan Emanuel, Alon Cohen, Aren Jansen, Harshvardhan Gazula, Gina Choe, Aditi Rao, Catherine Kim, Colton Casto, Fanda Lora, Adeem Flinker, Sasha Devore, Werner Doyle, Patricia Dugan, Daniel Friedman, Avinatan Hassidim, Michael Brenner, Yossi Matias, Ken A. Norman, Orrin Devinsky, and Uri Hasson. Thinking ahead: prediction in context as a keystone of language in humans and machines. *bioRxiv*, page 2020.12.02.403477, January 2021. . Publisher: Cold Spring Harbor Laboratory Section: New Results.
- Ari Holtzman, Jan Buys, Li Du, Maxwell Forbes, and Yejin Choi. The Curious Case of Neural Text Degeneration. *arXiv:1904.09751 [cs]*, February 2020. arXiv: 1904.09751.
- Sam Wiseman, Stuart M. Shieber, and Alexander M. Rush. Challenges in Data-to-Document Generation. *arXiv:1707.08052 [cs]*, July 2017. arXiv: 1707.08052.
- Nandan Thakur, Nils Reimers, Andreas Rücklé, Abhishek Srivastava, and Iryna Gurevych. BEIR: A Heterogeneous Benchmark for Zero-shot Evaluation of Information Retrieval Models. *arXiv:2104.08663 [cs]*, September 2021. arXiv: 2104.08663.
- Colin Raffel, Noam Shazeer, Adam Roberts, Katherine Lee, Sharan Narang, Michael Matena, Yanqi Zhou, Wei Li, and Peter J. Liu. Exploring the Limits of Transfer Learning with a Unified Text-to-Text Transformer. *arXiv:1910.10683 [cs, stat]*, July 2020. arXiv: 1910.10683.
- Kalpesh Krishna, Aurko Roy, and Mohit Iyyer. Hurdles to Progress in Long-form Question Answering. *arXiv:2103.06332 [cs]*, May 2021. arXiv: 2103.06332.
- Yair Lakretz, German Kruszewski, Theo Desbordes, Dieuwke Hupkes, Stanislas Dehaene, and Marco Baroni. The emergence of number and syntax units in LSTM language models. *arXiv:1903.07435 [cs]*, April 2019. arXiv: 1903.07435.
- Suhas Arehalli and Tal Linzen. Neural language models capture some, but not all, agreement attraction effects. 2020.
- Yair Lakretz, Theo Desbordes, Jean-Rémi King, Benoît Crabbé, Maxime Oquab, and Stanislas Dehaene. Can RNNs learn Recursive Nested Subject-Verb Agreements? *arXiv:2101.02258 [cs]*, January 2021. arXiv: 2101.02258.
- Marco Baroni. Linguistic generalization and compositionality in modern artificial neural networks. *Philosophical Transactions of the Royal Society B: Biological Sciences*, 375(1791): 20190307, February 2020. ISSN 0962-8436, 1471-2970. . arXiv: 1904.00157.
- Brenden M. Lake and Gregory L. Murphy. Word meaning in minds and machines. *arXiv:2008.01766 [cs]*, April 2021. arXiv: 2008.01766.
- Gary Marcus. Gpt-2 and the nature of intelligence. *The Gradient*, 2020.
- David E. Rumelhart and James L. McClelland. An interactive activation model of context

- effects in letter perception: II. The contextual enhancement effect and some tests and extensions of the model. *Psychological Review*, 89(1):60–94, 1982. ISSN 1939-1471. . Place: US Publisher: American Psychological Association.
22. Rajesh P. N. Rao and Dana H. Ballard. Predictive coding in the visual cortex: a functional interpretation of some extra-classical receptive-field effects. *Nature Neuroscience*, 2(1):79–87, January 1999. ISSN 1546-1726. . Bandiera_abtest: a Cg_type: Nature Research Journals Number: 1 Primary_atype: Research Publisher: Nature Publishing Group.
 23. Karl Friston and Stefan Kiebel. Predictive coding under the free-energy principle. *Philosophical Transactions of the Royal Society of London. Series B, Biological Sciences*, 364(1521):1211–1221, May 2009. ISSN 1471-2970. .
 24. Roel M. Willems, Stefan L. Frank, Annabel D. Nijhof, Peter Hagoort, and Antal van den Bosch. Prediction During Natural Language Comprehension. *Cerebral Cortex*, 26(6):2506–2516, June 2016. ISSN 1047-3211, 1460-2199. .
 25. Alessandro Lopopolo, Stefan L. Frank, Antal van den Bosch, and Roel M. Willems. Using stochastic language models (SLM) to map lexical, syntactic, and phonological information processing in the brain. *PLOS ONE*, 12(5):e0177794, May 2017. ISSN 1932-6203. . Publisher: Public Library of Science.
 26. Kayoko Okada, William Matchin, and Gregory Hickok. Neural evidence for predictive coding in auditory cortex during speech production. *Psychonomic Bulletin & Review*, 25(1):423–430, February 2018. ISSN 1531-5320. .
 27. Cory Shain, Idan Asher Blank, Marten van Schijndel, William Schuler, and Evelina Fedorenko. fMRI reveals language-specific predictive coding during naturalistic sentence comprehension. *bioRxiv*, page 717512, December 2019. . Publisher: Cold Spring Harbor Laboratory Section: New Results.
 28. Micha Heilbron, Benedikt Ehinger, Peter Hagoort, and Floris P. de Lange. Tracking Naturalistic Linguistic Predictions with Deep Neural Language Models. *2019 Conference on Cognitive Computational Neuroscience*, 2019. . arXiv: 1909.04400.
 29. Peter W. Donhauser and Sylvain Baillet. Two Distinct Neural Timescales for Predictive Speech Processing. *Neuron*, 105(2):385–393.e9, January 2020. ISSN 08966273. .
 30. Zahra Mousavi, Mohammad Mahdi Kiani, and Hamid Aghajan. Brain signatures of surprise in EEG and MEG data. Technical report, January 2020. Company: Cold Spring Harbor Laboratory Distributor: Cold Spring Harbor Laboratory Label: Cold Spring Harbor Laboratory Section: New Results Type: article.
 31. K. J. Forseth, G. Hickok, P. S. Rollo, and N. Tandon. Language prediction mechanisms in human auditory cortex. *Nature Communications*, 11(1):5240, October 2020. ISSN 2041-1723. . Bandiera_abtest: a Cc_license_type: cc_by Cg_type: Nature Research Journals Number: 1 Primary_atype: Research Publisher: Nature Publishing Group Subject_term: Cortex;Language;Neural encoding Subject_term_id: cortex:language;neural-encoding.
 32. Samuel A. Nastase, Yun-Fei Liu, Hanna Hillman, Asieh Zadbood, Liat Hasenfratz, Neggin Keshavarzian, Janice Chen, Christopher J. Honey, Yaara Yeshurun, Mor Regev, Mai Nguyen, Claire H. C. Chang, Christopher Baldassano, Olga Lositsky, Erez Simony, Michael A. Chow, Yuan Chang Leong, Paula P. Brooks, Emily Micciche, Gina Choe, Ariel Goldstein, Tamara Vanderwal, Yaroslav O. Halchenko, Kenneth A. Norman, and Uri Hasson. Narratives: fMRI data for evaluating models of naturalistic language comprehension. preprint, Neuroscience, December 2020.
 33. Charlotte Caucheteux, Alexandre Gramfort, and Jean-Rémi King. Disentangling Syntax and Semantics in the Brain with Deep Networks. *arXiv:2103.01620 [cs, q-bio]*, June 2021. arXiv: 2103.01620.
 34. Leila Wehbe, Ashish Vaswani, Kevin Knight, and Tom Mitchell. Aligning context-based statistical models of language with brain activity during reading. In *Proceedings of the 2014 Conference on Empirical Methods in Natural Language Processing (EMNLP)*, pages 233–243, Doha, Qatar, October 2014. Association for Computational Linguistics. .
 35. Alexander G. Huth, Wendy A. de Heer, Thomas L. Griffiths, Frédéric E. Theunissen, and Jack L. Gallant. Natural speech reveals the semantic maps that tile human cerebral cortex. *Nature*, 532(7600):453–458, April 2016. ISSN 0028-0836, 1476-4687. .
 36. Mariya Toneva, Tom M. Mitchell, and Leila Wehbe. The meaning that emerges from combining words is robustly localizable in space but not in time. preprint, Neuroscience, September 2020.
 37. Jacob Devlin, Ming-Wei Chang, Kenton Lee, and Kristina Toutanova. BERT: Pre-training of Deep Bidirectional Transformers for Language Understanding. *arXiv:1810.04805 [cs]*, May 2019. arXiv: 1810.04805.
 38. Yinhan Liu, Myle Ott, Naman Goyal, Jingfei Du, Mandar Joshi, Danqi Chen, Omer Levy, Mike Lewis, Luke Zettlemoyer, and Veselin Stoyanov. RoBERTa: A Robustly Optimized BERT Pretraining Approach. *arXiv:1907.11692 [cs]*, July 2019. arXiv: 1907.11692.
 39. Kevin Clark, Minh-Thang Luong, and Quoc V. Le. ELECTRA: PRE-TRAINING TEXT ENCODERS AS DISCRIMINATORS RATHER THAN GENERATORS. page 18, 2020.
 40. D. L. K. Yamins, H. Hong, C. F. Cadieu, E. A. Solomon, D. Seibert, and J. J. DiCarlo. Performance-optimized hierarchical models predict neural responses in higher visual cortex. *Proceedings of the National Academy of Sciences*, 111(23):8619–8624, June 2014. ISSN 0027-8424, 1091-6490. .
 41. Seyed-Mahdi Khaligh-Razavi and Nikolaus Kriegeskorte. Deep Supervised, but Not Unsupervised, Models May Explain IT Cortical Representation. *PLOS Computational Biology*, 10(11):e1003915, November 2014. ISSN 1553-7358. . Publisher: Public Library of Science.
 42. Umut Güçlü and Marcel A. J. van Gerven. Deep Neural Networks Reveal a Gradient in the Complexity of Neural Representations across the Ventral Stream. *Journal of Neuroscience*, 35(27):10005–10014, July 2015. ISSN 0270-6474, 1529-2401. . Publisher: Society for Neuroscience Section: Articles.
 43. Michael Eickenberg, Alexandre Gramfort, Gaël Varoquaux, and Bertrand Thirion. Seeing it all: Convolutional network layers map the function of the human visual system. *NeuroImage*, 152:184–194, May 2017. ISSN 10538119. .
 44. Charlotte Caucheteux, Alexandre Gramfort, and Jean-Rémi King. GPT-2's activations predict the degree of semantic comprehension in the human brain. *bioRxiv*, page 2021.04.20.440622, April 2021. . Publisher: Cold Spring Harbor Laboratory Section: New Results.
 45. Sam J. Gilbert and Paul W. Burgess. Executive function. *Current biology: CB*, 18(3):R110–114, February 2008. ISSN 0960-9822. .
 46. Tim Shallice and Paul Burgess. Deficits in strategy application following frontal lobe damage in man. *Brain : a journal of neurology*, 114 (Pt 2):727–41, May 1991. .
 47. Lin Wang. Dynamic predictive coding across the left fronto-temporal language hierarchy: Evidence from MEG, EEG and fMRI. page 29.
 48. Caroline S. Lee, Mariam Aly, and Christopher Baldassano. Anticipation of temporally structured events in the brain. *eLife*, 10:e64972, April 2021. ISSN 2050-084X. .
 49. Y. Lerner, C. J. Honey, L. J. Silbert, and U. Hasson. Topographic Mapping of a Hierarchy of Temporal Receptive Windows Using a Narrated Story. *Journal of Neuroscience*, 31(8):2906–2915, February 2011. ISSN 0270-6474, 1529-2401. .
 50. Charlotte Caucheteux, Alexandre Gramfort, and Jean-Rémi King. Model-based analysis of brain activity reveals the hierarchy of language in 305 subjects. In *EMNLP 2021 - Conference on Empirical Methods in Natural Language Processing*, Punta Cana (and Online), Dominican Republic, November 2021.
 51. Yamil Vidal, Perrine Brusini, Michela Bonfieni, Jacques Mehler, and Tristan A. Bekinschtein. Neural Signal to Violations of Abstract Rules Using Speech-Like Stimuli. *eNeuro*, 6(5), September 2019. ISSN 2373-2822. . Publisher: Society for Neuroscience Section: New Research.
 52. Matthew J. Nelson, Imen El Karoui, Kristof Giber, Xiaofang Yang, Laurent Cohen, Hilda Koopman, Sydney S. Cash, Lionel Naccache, John T. Hale, Christophe Pallier, and Stanislas Dehaene. Neurophysiological dynamics of phrase-structure building during sentence processing. *Proceedings of the National Academy of Sciences*, 114(18):E3669–E3678, May 2017. ISSN 0027-8424, 1091-6490. .
 53. Nai Ding, Lucia Melloni, Hang Zhang, Xing Tian, and David Poeppel. Cortical tracking of hierarchical linguistic structures in connected speech. *Nature neuroscience*, 19(1):158–164, 2016.
 54. Ray Jackendoff and Ray S Jackendoff. *Foundations of language: Brain, meaning, grammar, evolution*. Oxford University Press, USA, 2002.
 55. Cory Shain, Hope Kean, Benjamin Lipkin, Josef Afourtit, Matthew Siegelman, Francis Mollica, and Evelina Fedorenko. 'constituent length' effects in fMRI do not provide evidence for abstract syntactic processing. *bioRxiv*, 2021. .
 56. James L. McClelland and David E. Rumelhart. An interactive activation model of context effects in letter perception: I. An account of basic findings. *Psychological Review*, 88(5):375–407, 1981. ISSN 1939-1471. . Place: US Publisher: American Psychological Association.
 57. Christian Szegedy, Wei Liu, Yangqing Jia, Pierre Sermanet, Scott Reed, Dragomir Anguelov, Dumitru Erhan, Vincent Vanhoucke, and Andrew Rabinovich. Going deeper with convolutions. In *2015 IEEE Conference on Computer Vision and Pattern Recognition (CVPR)*, pages 1–9, Boston, MA, USA, June 2015. IEEE. ISBN 978-1-4673-6964-0. .
 58. Ting Chen, Simon Kornblith, Mohammad Norouzi, and Geoffrey Hinton. A Simple Framework for Contrastive Learning of Visual Representations. *arXiv:2002.05709 [cs, stat]*, June 2020. arXiv: 2002.05709.
 59. Kaiming He, Haoqi Fan, Yuxin Wu, Saining Xie, and Ross Girshick. Momentum Contrast for Unsupervised Visual Representation Learning. *arXiv:1911.05722 [cs]*, March 2020. arXiv: 1911.05722.
 60. Alaeldin El-Nouby, Hugo Touvron, Mathilde Caron, Piotr Bojanowski, Matthijs Douze, Armand Joulin, Ivan Laptev, Natalia Neverova, Gabriel Synnaeve, Jakob Verbeek, and Hervé Jegou. XCIT: Cross-Covariance Image Transformers. *arXiv:2106.09681 [cs]*, June 2021. arXiv: 2106.09681 version: 2.
 61. Adrien Bardes, Jean Ponce, and Yann LeCun. Vicreg: Variance-invariance-covariance regularization for self-supervised learning. *arXiv preprint arXiv:2105.04906*, 2021.
 62. Oscar Esteban, Christopher J. Markiewicz, Ross W. Blair, Craig A. Moodie, A. Ilkay Isik, Asier Erramuzpe, James D. Kent, Mathias Goncalves, Elizabeth DuPre, Madeleine Snyder, Hiroyuki Oya, Satrajit S. Ghosh, Jesse Wright, Joke Durnez, Russell A. Poldrack, and Krzysztof J. Gorgolewski. fMRIPrep: a robust preprocessing pipeline for functional MRI. *Nature Methods*, 16(1):111–116, January 2019. ISSN 1548-7105. .
 63. Thomas Wolf, Lysandre Debut, Victor Sanh, Julien Chaumond, Clement Delangue, Anthony Moi, Pierric Cistac, Tim Rault, Rémi Louf, Morgan Funtowicz, Joe Davison, Sam Shleifer, Patrick von Platen, Clara Ma, Yacine Jernite, Julien Plu, Canwen Xu, Teven Le Scao, Sylvain Gugger, Mariama Drame, Quentin Lhoest, and Alexander M. Rush. Transformers: State-of-the-art natural language processing. In *Proceedings of the 2020 Conference on Empirical Methods in Natural Language Processing: System Demonstrations*, pages 38–45, Online, October 2020. Association for Computational Linguistics.
 64. F. Pedregosa, G. Varoquaux, A. Gramfort, V. Michel, B. Thirion, O. Grisel, M. Blondel, P. Prettenhofer, R. Weiss, V. Dubourg, J. Vanderplas, A. Passos, D. Cournapeau, M. Brucher, M. Perrot, and E. Duchesnay. Scikit-learn: Machine learning in Python. *Journal of Machine Learning Research*, 12:2825–2830, 2011.
 65. Christophe Destrieux, Bruce Fischl, Anders Dale, and Eric Halgren. Automatic parcellation of human cortical gyri and sulci using standard anatomical nomenclature. *NeuroImage*, 53(1):1–15, October 2010. ISSN 1053-8119. .
 66. Paull Virtanen, Ralf Gommers, Travis E. Oliphant, Matt Haberland, Tyler Reddy, David Cournapeau, Evgeni Burovski, Pearu Peterson, Warren Weckesser, Jonathan Bright, Stéfan J. van der Walt, Matthew Brett, Joshua Wilson, K. Jarrod Millman, Nikolay Mayorov, Andrew R. J. Nelson, Eric Jones, Robert Kern, Eric Larson, C. J. Carey, Ilhan Polat, Yu Feng, Eric W. Moore, Jake VanderPlas, Denis Laxalde, Josef Perktold, Robert Cimrman, Ian Henriksen, E. A. Quintero, Charles R. Harris, Anne M. Archibald, António H. Ribeiro, Fabian Pedregosa, Paul van Mulbregt, and SciPy 1.0 Contributors. SciPy 1.0: Fundamental Algorithms for Scientific Computing in Python. *Nature Methods*, 17:261–272, 2020. .
 67. Zhilin Yang, Zihang Dai, Yiming Yang, Jaime Carbonell, Ruslan Salakhutdinov, and Quoc V. Le. XLNet: Generalized Autoregressive Pretraining for Language Understanding. *arXiv:1906.08237 [cs]*, January 2020. arXiv: 1906.08237.
 68. Zihang Dai, Zhilin Yang, Yiming Yang, Jaime Carbonell, Quoc V. Le, and Ruslan Salakhutdinov. Transformer-XL: Attentive Language Models Beyond a Fixed-Length Context. *arXiv:1901.02860 [cs, stat]*, June 2019. arXiv: 1901.02860.

Supporting Information (SI)

M. Generalisation to other architectures. The analyses in the main manuscript focus on one representative deep neural network: GPT-2 (2). Here, we replicate our results with the activations extracted from seven other transformer architectures. We only analyse *causal* models, trained to predict a word from their *previous* context[§]. Similarly as with GPT-2, we use the pretrained models from Huggingface (labeled ‘distilgpt2’, ‘gpt2’, ‘gpt2-medium’, ‘gpt2-large’, ‘gpt2-large’, ‘gpt2-xl’, ‘transfo-xl-wt103’, ‘xlnet-base-cased’, ‘xlnet-large-cased’), based on GPT-2 (2), XLNet (67) and Transformer-XL (68) architectures, and focus on one intermediate-to-deep layer of the model ($l = \frac{2}{3} \times n_{\text{layers}}$). For each architecture, we 1) extract the activations corresponding to the subjects’ stories (Methods C) 2) compute the corresponding brain scores (Methods D) and forecast scores (Methods F) for each voxel, subject, and forecast distance. As displayed in Figure S5, the seven architectures accurately map onto brain activity (Figure S5A), and the mapping is improved when adding information about around eight words in the future (Figure S5B). The mapping is also improved when adding representations of words automatically generated by GPT-2 instead of the true future words (we use sampling methods to generate words, similarly as in SI.N).

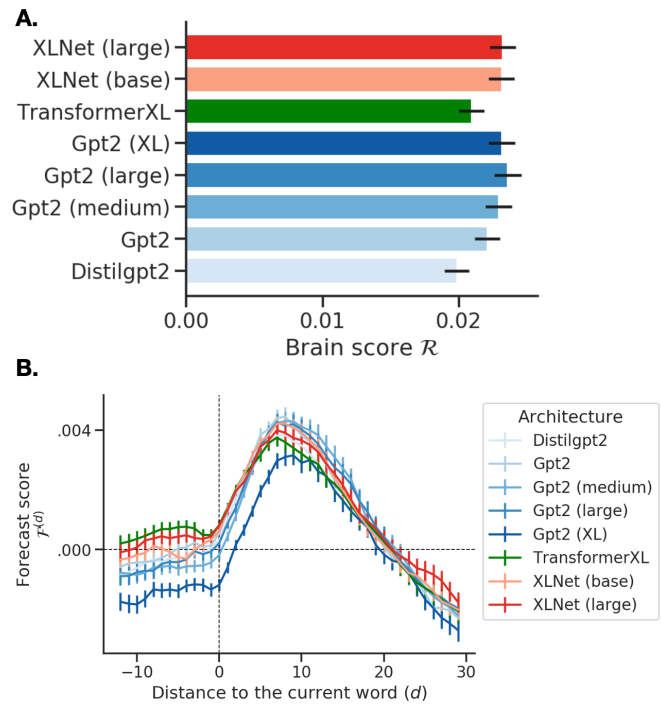


Fig. S5. Generalisation to other architectures. **A.** Brain scores (cf. Figure 1B, Methods D) of eight transformer models, based on XLNet (67), TransformerXL (68) and GPT-2 (2) architectures. We use the pre-trained models from Huggingface and proceed similarly as with GPT-2 (Methods C). Brain scores are averaged across voxels and subjects, error bars are the standard errors of the mean across subjects. **B.** Same as Figure 2D for the eight transformer architectures.

N. Controls.

[§]Note that XLNet is trained to predict both left and right context (67), but, here, we only input the model with left context when extracting the activations.

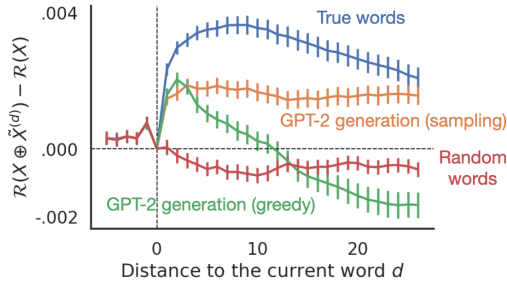


Fig. S6. Controls. Forecast scores for different types of forecast representations \tilde{X} . Here, we use a growing window analysis: $\tilde{X}^{(d)}$ is the concatenation of the activations of $|d|$ future ($d > 0$) or past ($d < 0$) words; the size of the window thus varies with the distance. The forecast score is the gain in brain score when concatenating the forecast window (cf. Eq. (3)). In blue, \tilde{X} is built out of the true words of the story. In red, \tilde{X} is built out of randomly picked words from all stories. In green and orange, \tilde{X} is built out of words generated by GPT-2. Precisely, GPT-2 is input with the current word and its previous context, and we use greedy (green) and sampling (orange) decoding schemes to generate a sequence of expected words. For simplicity, when $d < 0$, \tilde{X} is the concatenation of d true past words. When $d > 0$, \tilde{X} is the concatenation of d future words (either true, generated or random words).

Testing different window sizes In the previous paragraphs, we use a sliding forecast window with a *fixed* number of words in order to compare the brain scores of representations with the same dimensionality. Here, we test different window sizes by implementing a growing window analysis. Precisely, we build the forecast window $\tilde{X}^{(d)}$ by concatenating the d words succeeding the current word. The size of the window thus varies and d corresponds to both the number of words in the window, and the distance between the last word and the current word. We proceed similarly as in the main manuscript, build forecast window for different distances d and the corresponding forecast scores. As displayed in Figure S6, the forecast score is maximal for a window of 8 future words ($d^* = 7.9 \pm 0.5$ on average across subjects), which is consistent with the previous results (Figure 2C, where $d^* = 8$).

Using random forecast representations We use the same growing window framework and check that adding a forecast window composed of random words does not improve the brain score (Figure S6). Precisely, we randomly pick words out of all stories, concatenate the GPT-2 activations of random words to build the forecast windows $\tilde{X}^{(d)}$, and compute the corresponding forecast scores for different distances d . Figure S6 shows that random forecast windows do *not* improve our ability to predict brain activity.

Using GPT-2 generations as forecast representations To what extent are the improvements in brain score due to (1) additional information about future words and/or (2) a different way to represent past words? To address this question, we repeat the same analysis with a forecast window input, not of the *true* future words, but with the words *generated* by GPT-2. Specifically, for each word w_k , we 1) input GPT-2 with its past context w_0, \dots, w_k , 2) generate future words $w'_{k+1}, \dots, w'_{k+n}$ using different decoding methods (greedy and sampling schemes[¶] (10)), 3) extract the corresponding activations $X'_{k+1}, \dots, X'_{k+n}$, 4) build the growing windows from these activations and 5)

compute their forecast scores. Thus, the brain signals, the current activations X_k and the activations of generated words $X'_{k+n} \dots X'_{k+n}$ are all distinct transformations of the same past words w_0, \dots, w_k . The results show that a window made of *generated* words improves the brain score, although less so than a window made of the *true* words of the stories (Figure S6), confirming that GPT-2 is an imperfect forecaster.

O. Shared-Response-Model *a.k.a* “Noise ceiling”. fMRI recordings are inherently noisy. To assess the amount of explainable signal, we use a shared-response-model, *i.e.* we predict the brain responses of one subject given the other subjects’ responses to the same story. Precisely, for one subject s and voxel v , we apply the exact same setting as Eq. (1), but use the average brain signals of other subjects’ brain $\bar{Y}^{(s)} = \frac{1}{|\mathcal{S}|} \sum_{s' \neq s} Y^{(s')}$ (of size $T \times V$) instead of the network’s activations X . Thus, the ‘noise ceiling’ of one subject s and voxel v evaluated on one test set I , is given by:

$$\text{Corr}(W \cdot \bar{Y}^{(s)}, Y^{(s,v)}) \quad , \quad [8]$$

with Corr Pearson’s correlation and W a ℓ_2 -penalized linear regression fitted on separate train data, following the notation of Eq. (1). The noise ceilings are computed on five test folds using a cross-validation scheme across time samples and averaged across the five test folds, following the exact same framework as in Methods D. Results are displayed in Figure S7. This score is one possible upper bound for the best brain score that can be obtained given the level of noise in the dataset.

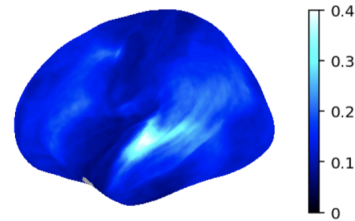


Fig. S7. Shared response model Noise ceiling estimates averaged across subjects, for each voxels of the left hemisphere (SI. O).

P. Scores per region of interest. For clarity, we report below (Figure S8) the average brain scores, forecast scores, forecast distances and depths for each region of interest in both the left and right hemispheres.

[¶]Using Huggingface’s sampling scheme with `topk=50` and `topp=0.95`, `do_sample=True`, `max_length=100`. For the greedy scheme, we simply set `do_sample` to `False`, `topk` and `topp` to 1.

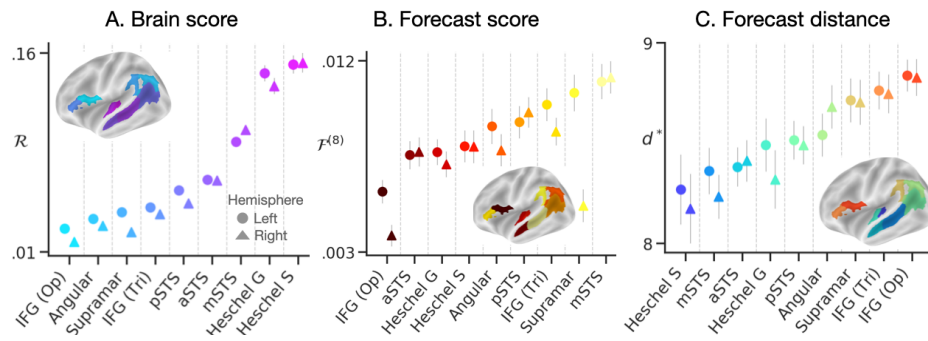


Fig. S8. Scores per region of interest. A-E. Brain scores (Figure 2A, Methods D), forecast scores (Figure 2C, Methods F), forecast distance (Figure 2E Methods G) and forecast depth (Figure 3A, Methods H) for nine regions of interests in both the left (circle) and right (triangle) hemispheres. Scores are averaged across voxels within each region of interest and across subjects. Error bars are the standard errors of the mean across subjects. Regions are ordered with respect to their average score in the left hemisphere.